

# Co-published by Institute of Fluid-Flow Machinery Polish Academy of Sciences

## **Committee on Thermodynamics and Combustion**

Polish Academy of Sciences

Copyright@2025 by the Authors under licence CC BY-NC-ND 4.0

http://www.imp.gda.pl/archives-of-thermodynamics/



# Integrated model of a biomass boiler coupled with a Stirling engine

Javier Uche<sup>a\*</sup>, Sergio Usón<sup>b</sup>, Juan Anat Gómez<sup>c</sup>

<sup>a</sup> ENERGAIA Institute and Department of Mechanical Engineering, University of Zaragoza. Mariano Esquillor 15, 50018 Zaragoza, Spain
 <sup>b</sup> ENERGAIA Institute and Department of Mechanical Engineering, University of Zaragoza. Maria de Luna 5, 50018 Zaragoza, Spain
 <sup>c</sup> ENERGAIA Institute, University of Zaragoza. Mariano Esquillor 15, 50018 Zaragoza, Spain
 \*Corresponding author email: javiuche@unizar.es

Received: date here; revised: date here; accepted: date here

# **Abstract**

Integration of a Stirling engine in a biomass boiler can be an interesting renewable alternative for the supply of heat and electricity in isolated homes located in areas where local biomass is available and during months when sunlight is low. Since this integration requires a careful coupling of the engine and boiler, an integrated model of these two devices is a relevant issue. In this case, a modular integrated model of a 25 kW<sub>th</sub> biomass pellet boiler, fire-tube with a cylindrical water jacket, coupled to a 1 kW<sub>e</sub> free piston Stirling engine is presented. To model the boiler, and take into account the location of the Stirling head, the zonal method was chosen, which allows estimating this temperature from an additional set of surrounding temperatures. For the Stirling engin, a model widely used to evaluate those engines was used. Various software tools have been used to integrate the model sequentially. The integrated model predicts the thermal and electrical production based on different operation parameters, such as the boiler load in 5% fractions of its load from 50 to 100%. The obtained results, which will be validated with the experimental setup, show a maximum output of approximately 600 W for the engine and a decreasing temperature profile in the combustion chamber, as a function of the partial load.

**Keywords:** Biomass boiler; Stirling engine; Integrated systems; Energy modelling; Cogeneration

Vol. 46(2025), No. 2, 133-141; doi: 10.24425/ather.2025.154912

Cite this manuscript as: Uche, J., Usón, S., & Gómez, J.A. (2025). Integrated model of a biomass boiler coupled with an Stirling engine. *Archives of Thermodynamics*, 46(2), 133–141.

### 1. Introduction

In the field of combined heat and power generation in the form of cogeneration, integrating a domestic biomass boiler (BB) with a Stirling engine (SE) allows for the provision of both demands [1,2]. It may be enough to meet the needs of a household, especially in isolated areas where biomass is available in certain abundance and where, in many cases, the power grid supply may be distant. Unfortunately, the high investment costs of Stirling technology make it scarcely competitive compared to other technologies, such as photovoltaics (PV). Still, it can be a cost-effective option in cold areas with low electricity demand and high

heat demand for heating and domestic hot water. Alternatively, this technology may be the only feasible option in areas with low solar insolation and limited space availability for placing PV panels. Finally, the proposed scheme may complement solar energy by operating in winter when radiation is low.

The research focused on modelling and improving SE remains relevant [3] within a power range from 1 to 225 kW<sub>e</sub>. Free piston type Stirling engine (FPSE), due to its simplicity in transmission, long operating life, low sound pollution and high efficiency, is usually selected as SE [4]. Anyway, it is very complex to design, and its start-up is also complex. Its performance has been studied in-depth for diverse typologies [5], and its efficie-

## **Nomenclature**

a – weight coefficient (WSGG model)

A − area, m<sup>2</sup>

c – coefficient associated to the k value (WSGG model)

 $c_p$  – specific heat, J/(kg·K)

d – hydraulic diameter, m

D – diameter of the combustion chamber, m

E – emissive power, W/m<sup>2</sup>

f - frequency, Hz

 $f_r$  – friction coefficient

G – mass flow rate of the working fluid, kg/s

gg – gas-gas DEA matrix

GG – gas-gas TEA matrix

 $\overrightarrow{G_1G_1}$  – gas-gas DFA matrix

 $\overline{\mathbf{G_1}\mathbf{S_1}}$  gas-surface DFA matrix

h – heat transfer coefficient, W/(m<sup>2</sup>·K)

k − absorption coefficient of the WSGG model, m<sup>-1</sup>

l – length, m

m - mass stored, kg

M - mass (in SE), kg

Nu – Nusselt number

P - pressure, Pa

Pr - Prandtl number

Q - heat rate, W

R – specific gas constant of helium (2078 J/kg·K)

 $\overline{\mathbf{R}}$  – auxiliary matrix for TEA calculations

Re - Reynolds number

**<u>sg</u>** – surface-gas DEA matrix

**SG** – surface-gas TEA matrix

**SS** – surface-surface DEA matrix

**SS** – surface-surface TEA matrix

 $S_1S_1$  – surface-surface DFA matrix

T - temperature, K

V – volume,  $m^3$ 

### **Greek symbols**

 $\varepsilon$  – emissivity, effectiveness

 $\eta$  - thermal efficiency

 $\theta$  – crank angle, rad

 $\lambda$  – conductivity, W/(m·K)

 $\mu$  – viscosity, Pa·s

 $\rho$  – reflectivity

 $\sigma$  – Stefan-Boltzmann constant, 5.67·10<sup>-8</sup> W/(m<sup>2</sup>·K<sup>4</sup>)

## **Subscripts and Superscripts**

c – compression

cb – combustion

cv - convection

e - expansion, electrical

i - zone

g – gases (in the combustion chamber)

h – exhaust gases (inside of water jacket), heater

i – zone, volume

*j* – zone, volume

k - cooler

n - grey gas number

p – internal wall

r - regenerator

rd – radiation

s – surface

th – thermal

w - water, wetted, wall

## **Abbreviations and Acronyms**

BB – biomass boiler

 $\mu CHP-$  micro combined heat and power

DEA - direct exchange areas (matrix)

DFA - directed flux areas (matrix)

EES - Engineering Equation Solver

FPSE- free-piston Stirling engine

LHV – lower heating value

ORC – organic Rankine cycle

PL - part load operation

PV - photovoltaics

SE - Stirling engine

TEA – total exchange areas (matrix)

WSGG- weighted sum of grey gases (model)

ncy varied from 3% to 41% depending on the applied model. Hybrid SE-PV systems could considerably reduce CO<sub>2</sub> emissions by up to 69% compared with diesel generators [6]. A model of 3.9 kW<sub>e</sub> to be supplied by biomass or solar energy is presented in [7] and considered a renewable energy source. Using waste heat from SE to feed an Organic Rankine Cycle (ORC) in a cascade improves the SE performance by 63% to 66% [8]. In some cases, a program has been implemented that allows the design to be modified and the SE model to be selected to calculate its performance. However, it requires a lot of information [9]. Despite its limited commercialization and, therefore, confidentiality in the design, there are experiences of experimental validation for diverse but limited sizes. In [10], a 4.03 kW engine was optimized by combining the model and the performed tests. On the contrary, in [11], less than 1 W was tested in a small SE with also reduced efficiencies (6%). Typically, SE is powered by heat from fossil fuels. Integrated micro combined heat and power (µCHP) unit with an SE and a natural

gas boiler has been studied in terms of modelling and experimentation [12], providing up to 1 kW<sub>e</sub> for domestic boilers. In [13], the overall efficiency of the  $\mu$ CHP unit was close to 100% based on the LHV by using an SE with N<sub>2</sub>.

There is hardly any scientific literature on the subject of integration of a BB feeding a SE. The main works are those of Choque and Araoz [14] and Cardozo et al. [15]. Both papers analyse a 1 kW<sub>e</sub> SE coupled with a 20 or 30 kW BB. However, SE is a two-cylinder of a gamma type, and the heater is made of tubes, which is somewhat different than our SE. Damirchi et al. [16] tested diverse biomass and obtained 96 W by a small gamma type SE. Arashnia et al. [17] used the same gamma type SE but modified the previous simple BB, with similar results of low power obtained in the engine (< 100 W). This first research group has also carried out a validation with an integrated model of experiments of BB with SE [18,19]. In any case, the boiler model is able to estimate the performance but does not detail aspects of its design, which may affect a better capture of heat

to obtain a maximum electrical production in the engine, as well as avoiding as far as possible the formation of ash deposits in its head.

Therefore, and after the humble analysis by the authors of the state-of-the-art integrated model of a BB with an SE, it has been found that there is no such model, at least with a similar level of detail in both pieces of equipment. An integrated, modular and flexible model that allows us to analyze the variations in certain design parameters of the biomass boiler, and to see how they affect the production and reliable operation of SE constitutes a novelty.

In this article, both BB and SE are modelled sequentially. First, the model of BB is used to obtain temperature values, particularly in the area where the heat receiver is located, which in turn is used by the SE model to estimate the expected performance of the engine. Accordingly, the integrated model aims to estimate the expected production of heat and electricity from both units, which will later be tested in an already-constructed experimental facility.

## 2. Materials and methods

The modelled BB is a commercial unit of 25 kW $_{th}$  with a somewhat particular configuration (BioCurve BCH25). It is a fire tube, with the combustion gases from the combustion chamber circulating inside the tubes within a cylindrical water jacket. This boiler has the advantage of condensing water vapour of flue gases, which increases its efficiency, and has a system for cleaning the gas circuit with water.

As for SE, the approximate model basis is a 1 kW $_{\rm e}$  Free-Piston Stirling Engine (FPSE), whose working fluid is helium (Microgen/MEC, biomass Stirling converter). Its approximate operating range is for temperatures of its heat source around 180–550°C. Figure 1 shows the diagram of the experimental facility supporting the developed models. It should be noted that, in order to increase the efficiency of SE, it has an independent cooling system. Different software tools have been used for the model, taking advantage of each of their capabilities to make it more flexible.

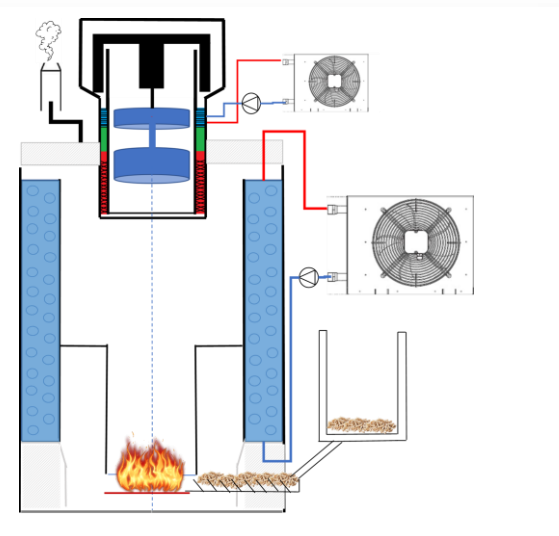
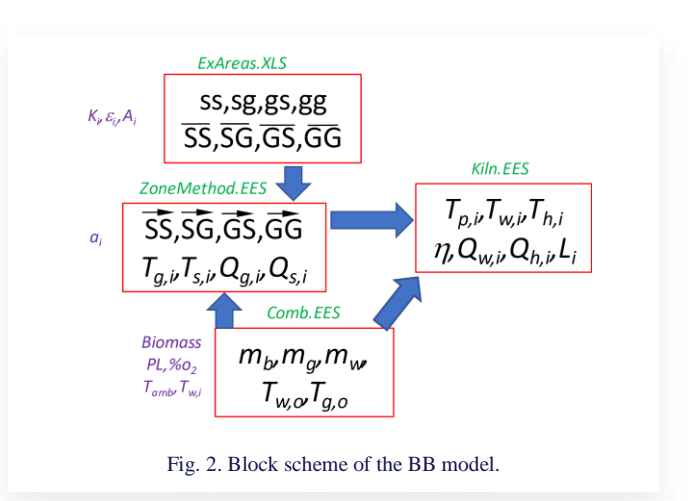
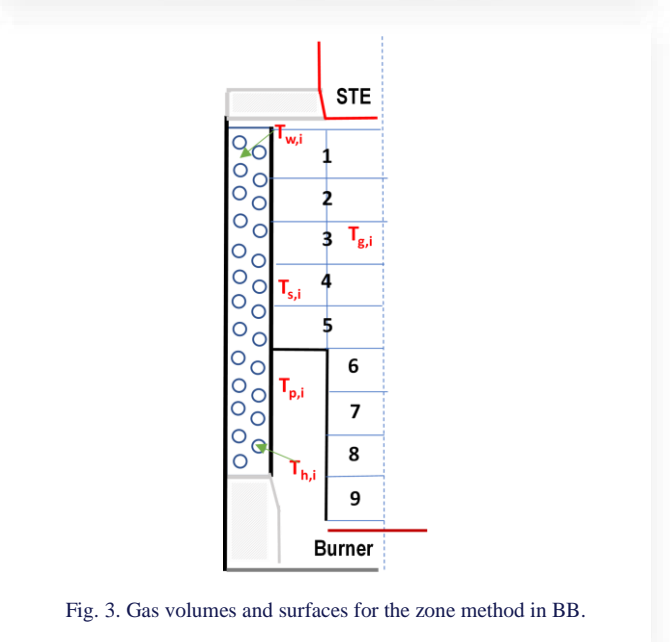


Fig. 1. Experimental facility of the hybrid BB+SE system.

#### 2.1. Biomass boiler model

The following Fig. 2 shows the conceptual diagram of the sequenced sub-models used to solve this BB model. In the end, thirteen temperatures of the inner surface  $(T_{s,i})$ , nine temperatures of gases  $(T_{g,i})$ , eight of exhaust gases and water inside the jacket  $(T_{h,i}, T_{w,i})$ , and other less relevant eight internal temperatures are obtained  $(T_{p,i})$ . One of the temperatures corresponds to the approximate location of the SE head placed in a vertical position, which will be crucial for examining the performance of the engine under partial load conditions of the boiler. The position of SE in the upper part of the boiler can be seen in Figs. 1 and 3. In the experimental facility, a lifting mechanism has been introduced that allows removing the engine quickly to prevent its overheating in case of a safety trip in the boiler or the engine itself. It should be noted that a metallic piece of cylindrical shape was located in the inner part of the commercial boiler to redirect gas flow towards the water jacket, but it has been removed to introduce the SE heater; accordingly, this piece is not present in the model.





The heat rate provided by combustion and gas flow, as well as the circulating water flow rate, were provided by a model created by the Engineering Equation Solver (EES) using data from an average pellet fuel composition in Spain [20] (see Table 1) and excess of air, giving the efficiency at partial loads adjusted to the offering of around 30 biomass boiler models available on the market, where condensation is only offered in rare situations.

The zonal method with nine gas zones ( $T_{g,i}$ ) and thirteen surfaces ( $T_{s,i}$ ) has been developed to estimate the net radiative balance in the combustion chamber, as detailed in Fig. 3.

Table 1. Biomass averaged composition.

Chemical element	% (or kJ/kg)
С	45.4
Н	5.755
N	0.087
S	0.1293
Cl	0.0054
0	40.94
W	7.628
LHV (dry basis)	17 566

The direct and total exchange areas were obtained using matrix algebra tools in Excel. Regarding the direct exchange areas (DEA), given the purely cylindrical geometry of this boiler in its simplification, the values available in Appendix 7 of the reference book on the subject [21] have been used. Based on the previously obtained DEA (surface-surface  $\overline{ss}$ , surface-gas  $\overline{sg}$  and gas-gas  $\overline{gg}$ ) and the emissivities  $\varepsilon$ , reflectivities  $\rho$  and areas A of each enclosure surface, an equation for the total exchange areas (TEA)  $\overline{SS}$ ,  $\overline{SG}$ ,  $\overline{GG}$  can be seen in the following Eqs. (1) to (4) by using matrix algebra [22]:

$$\overline{SS} = \varepsilon AI \cdot R \cdot \overline{SS} \cdot \varepsilon I, \tag{1}$$

$$\overline{SG} = \varepsilon AI \cdot R \cdot \overline{Sg}, \tag{2}$$

$$\overline{\mathbf{G}\mathbf{G}} = \overline{\mathbf{g}\mathbf{s}} \cdot \rho \mathbf{I} \cdot \mathbf{R} \cdot \overline{\mathbf{s}\mathbf{g}} + \overline{\mathbf{g}\mathbf{g}}, \tag{3}$$

$$\mathbf{R} = [\mathbf{A}\mathbf{I} - \overline{\mathbf{s}}\overline{\mathbf{s}} \cdot \boldsymbol{\rho}\mathbf{I}]^{-1}. \tag{4}$$

Subsequently, a second EES file performs the net radiative balance of the gas zones and interior surface zones of the combustion chamber, using the direct flux areas (DFA) based on the gas or surface temperatures and applying the Weighted Sum of Grey Gases (WSGG) model, which includes soot and particles due to biomass combustion, as described in [22]. The DFA  $\overline{S_1S_j}$ ,  $\overline{G_1S_j}$ ,  $\overline{G_1G_j}$  can be obtained for a grey-diffuse gas zone i or a surface i as a function of the abovementioned TEA for each attenuation coefficient  $k_{g,n}$  of the WSGG model, as follows in Eqs. (5) to (7):

$$\overline{\mathbf{S}_{\mathbf{i}}}\overrightarrow{\mathbf{S}_{\mathbf{j}}} = \sum_{n=1}^{N_g} a_{s,n}(T_i) \cdot (\overline{\mathbf{S}}\overline{\mathbf{S}})_{k=k_{g,n}}, \tag{5}$$

$$\overrightarrow{\mathbf{G_i}}\overrightarrow{\mathbf{S_j}} = \sum_{n=1}^{N_g} a_{g,n} (T_{g,i}) \cdot (\overline{\mathbf{G}}\overrightarrow{\mathbf{S}})_{k=k_{g,n}}, \tag{6}$$

$$\overrightarrow{\mathbf{G}_{\mathbf{I}}\mathbf{G}_{\mathbf{J}}} = \sum_{n=1}^{N_g} a_{g,n} (T_{g,i}) \cdot (\overline{\mathbf{G}\mathbf{G}})_{k=k_{g,n}}. \tag{7}$$

The previously mentioned  $a_{s,n}$  or  $a_{g,n}$  weight coefficients for the WSGG model used are presented in Eqs. (8) and (9):

$$a_i = \sum_{j=1}^{N_c} c_{i,j} \left(\frac{T}{T_{ref}}\right)^{j-1},$$
 (8)

$$a_{i=0} = 1 - \sum_{i=1}^{N_g} a_i. (9)$$

The four  $k_{g,n}$  values in the WSGG model are 0 (transparent), 0.2715, 2.5005 and 39.1395 m<sup>-1</sup>, respectively, each one including five  $c_{i,j}$  coefficients [23], the reference temperature for normalization  $T_{ref}$  being equal to 1200 K.

Therefore, the net radiative balance for the case of a surface  $A_i$  is presented in Eqs. (10) and (11), where  $E_i$  is the emissive power of the surface  $A_i$ :

$$\sum_{j=1}^{m} \overrightarrow{S_{l}S_{j}} \cdot E_{j} + \sum_{j=1}^{l} \overrightarrow{G_{j}S_{i}} \cdot E_{g,j} - A_{i} \cdot \varepsilon_{i} \cdot E_{i} = Q_{rd,i}, (10)$$

$$E_i = \sigma \cdot T_i^4. \tag{11}$$

The energy balance of a volume zone  $V_i$  is then presented in Eqs. (12) and (13), where  $E_{g,i}$  is the emissive power of the gas volume i:

$$\sum_{i=1}^{l} \overrightarrow{G_i} \overrightarrow{G_i} \cdot E_{g,j} + \sum_{i=1}^{l} \overrightarrow{S_i} \overrightarrow{G_i} \cdot E_j +$$

$$-4 \cdot \sum_{n=1}^{N_g} a_{g,n} \cdot k_{g,n} \cdot V_i \cdot E_{g,i} = Q_{rd,i},$$
 (12)

$$E_{q,i} = \sigma \cdot T_{q,i}^4. \tag{13}$$

Finally, in this section, the energy balance (heat rate Q in steady state) of a gas zone i is formulated as in [24], including the energy from the combustion (if proceed), the one of the gas flow at the inlet and outlet of the volume, convection with the walls, and further conduction losses to the outside of the boiler, see Eq. (14):

$$Q_{cb} + Q_{rd,i} - Q_{cv,i} + Q_{g,i} - Q_{g,i-1} = 0. (14)$$

The term related to convection is calculated as follows in Eqs. (15) and (16), where h, Nu, Re,  $\lambda$ , Pr and D are the convection coefficient, Nusselt number, conductivity, Prandtl number and diameter of the combustion chamber, respectively:

$$Q_{cv,i} = h_i \cdot A_i \cdot (T_{a,i} - T_{s,i}), \tag{15}$$

$$h_i = \frac{\text{Nu}_i \cdot \lambda}{D} = \frac{0.023 \cdot \text{Re}^{0.8} \cdot \text{Pr} \cdot \lambda}{D}.$$
 (16)

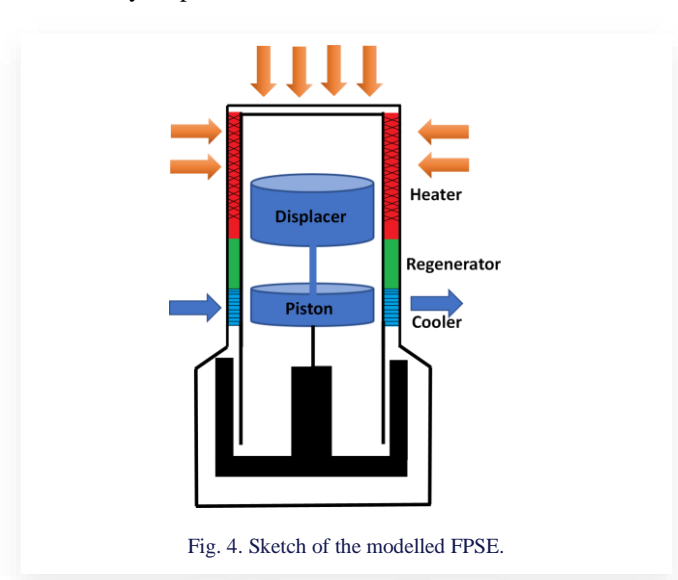
A simpler balance was also used for any surface  $A_I$ , considering that radiation and convection are transferred by conduction toward the water jacket.

Once the energy balance of the combustion chamber is completed, the fourth EES sub-model performs the energy balance in the internal walls  $(T_{p,i})$ , water jacket  $(T_{w,i})$ , exhaust gases inside of the jacket  $(T_{h,i})$  and the lower enclosure between the area closest to the burner and the water jacket, which has a passage section reduced by half due to a metallic piece in the boiler (already included in  $T_{p,i}$  or  $T_{s,i}$ ). The input data for this latest boiler sub-model uses the inner surface temperature profile from the radiative model and gas temperature  $T_{g,l}$ . An energy balance closure is considered when the boiler inputs and outputs (losses in gases, walls heat rate transferred to water) are less than 50 W: if not, some boiler design parameters are modified (emissivities,

generally, in some areas) and the Excel-3 EES simulation sequence is repeated.

## 2.2. Stirling engine model

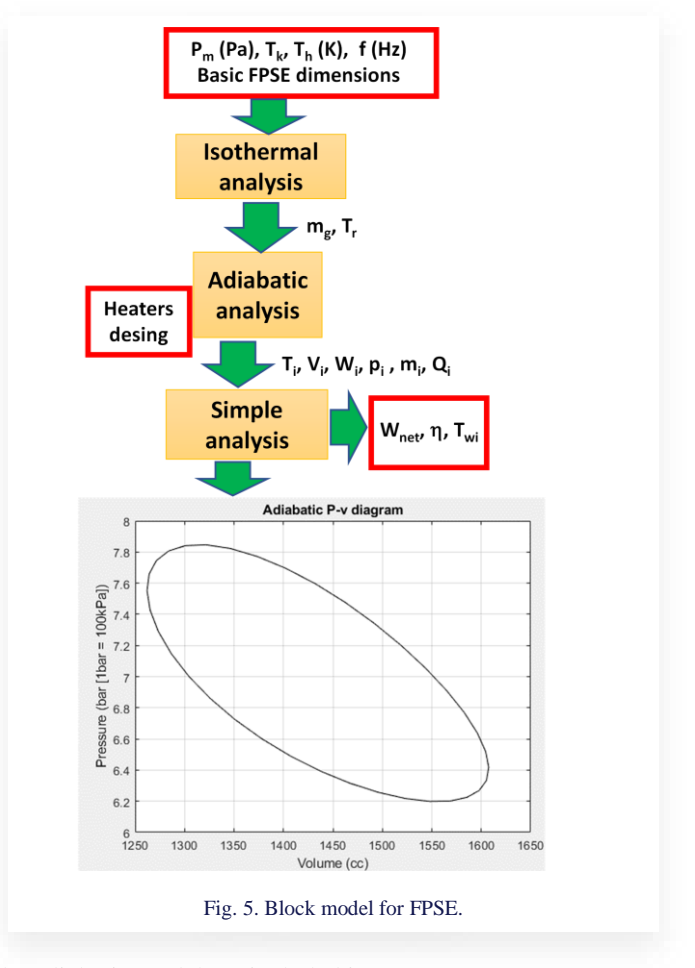
To model FPSE is a quite complex issue, as its integrated operation of the piston and displacer on the same axis, to avoid the crankshaft mechanism present in other types of SE  $(\alpha, \gamma)$ , requires a dynamic model considering the characteristics of the springs and dampers that make it up [25]. Anyway, such models are related to the design of SEs rather than the analysis of their performance. In this work, the most interesting aspect is to predict the electrical generation considering the heat rate provided by the boiler according to its regime. Thus, the three well-known thermodynamic models sequentially presented by Urieli and Berchowitz [26] have been adapted from the available code implemented in MATLAB [27] and tested for some commercial SE. Figure 4 shows a schematic of the free piston Stirling engine, but placed vertically upwards, and Fig. 5 shows the sequential model developed to further integrate it with BB. The program provides both overall power and performance values, as well as cycle parameters.



The model starts with the most basic scheme (Schmidt isothermal model) that provides an initial estimation of power, cycle efficiency, average working pressure and gas mass required in the cycle. Previously, the dimensions of the engine and working fluid were requested for preliminary analysis.

The second model includes a more realistic situation. Now, the compression and expansion processes are not considered isothermal but adiabatic. This implies a reduction in the efficiency of the thermodynamic cycle. The model already has a certain complexity, including solving a differential, incremental and conditioned equations system, which can be solved relatively quickly using the Runge-Kutta method.

The system consists of twenty-two variables and sixteen derivatives to be solved in a complete cycle ( $\theta = 0-2\pi$  rad), including seven derivatives that must be integrated numerically ( $T_c$ ,  $T_e$ ,  $Q_k$ ,  $Q_r$ ,  $Q_h$ ,  $W_c$ ,  $W_e$ ), nine variables that are analytical derivatives ( $W_r$ ,  $W_r$ ,



the adiabatic model are included in Eqs. (17) to (47).

First, Eqs. (17) and (18) are for pressure calculation and its variation in SE:

$$p = M \cdot R / \left( \frac{V_c}{T_c} + \frac{V_k}{T_k} + \frac{V_r}{T_r} + \frac{V_h}{T_h} + \frac{V_e}{T_e} \right), \tag{17}$$

$$dp = \frac{-\gamma \cdot p(\frac{dV_c}{T_{ck}} + \frac{dV_e}{T_{he}})}{\frac{V_c}{T_{ck}} + \gamma(\frac{V_k}{T_k} + \frac{V_r}{T_r} + \frac{V_h}{T_h}) + \frac{V_e}{T_{he}}}.$$
(18)

Equations (19) to (23) are related to mass calculations in the five volumes of SE:

$$m_c = \frac{p \cdot V_c}{R \cdot T_c},\tag{19}$$

$$m_k = \frac{p \cdot V_k}{R \cdot T_k},\tag{20}$$

$$m_r = \frac{p \cdot V_r}{R \cdot T_r},\tag{21}$$

$$m_h = \frac{p \cdot V_h}{R \cdot T_h},\tag{22}$$

$$m_e = \frac{p \cdot V_e}{R \cdot T_e}. (23)$$

Alternatively, Eqs. (24) to (28) estimate the mass accumulations in those five volumes:

$$dm_c = \frac{p \cdot dV_c + V_c \cdot dp/\gamma}{R \cdot T_{ck}},\tag{24}$$

$$dm_e = \frac{p \cdot dV_e + V_e \cdot dp/\gamma}{R \cdot T_{he}},$$
 (25)

$$dm_k = m_k \cdot \frac{dp}{p},\tag{26}$$

$$dm_r = m_r \cdot \frac{dp}{n},\tag{27}$$

$$dm_h = m_h \cdot \frac{dp}{p}. (28)$$

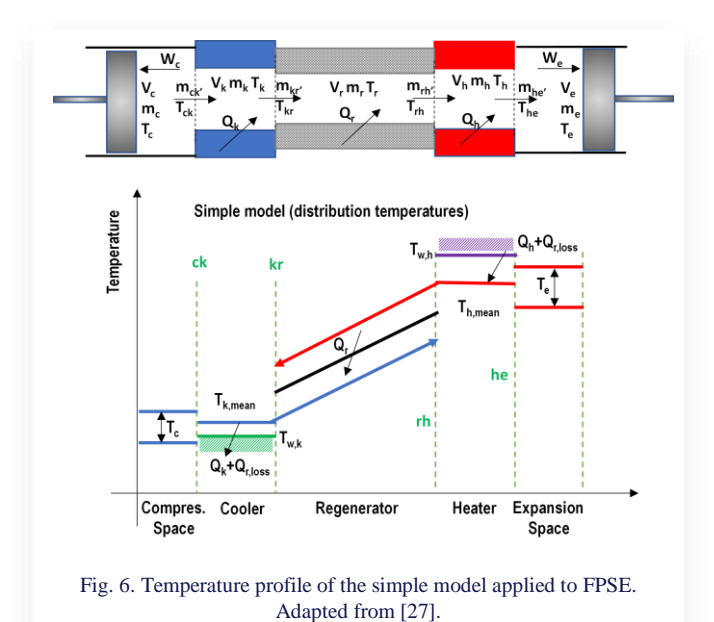
The mass flow rates between the five volumes of SE are shown in Eqs. (29) to (32); see Fig. (6) for details:

$$m_{ckl} = -dm_c, (29)$$

$$m_{kr\prime} = m_{ck\prime} - dm_k, \tag{30}$$

$$m_{he'} = dm_e, (31)$$

$$m_{rh'} = m_{he'} + dm_h. (32)$$



Temperatures in the SE interfaces (compression-cooler and heater-expansion) are calculated depending on the mass flow rate sense, according to Eqs. (33) and (34):

if 
$$m_{ckl} > 0$$
 then  $T_{ck} = T_c$  else  $T_{ck} = T_k$ , (33)

if 
$$m_{hel} > 0$$
 then  $T_{he} = T_h$  else  $T_{he} = T_e$ . (34)

Then, the evolution of the temperatures in the compression and expansion volumes is estimated in Eqs. (35) and (36):

$$dT_c = T_c \cdot \left(\frac{dp}{p} + \frac{dV_c}{V_c} - \frac{dm_c}{m_c}\right), \tag{35}$$

$$dT_e = T_e \cdot \left(\frac{dp}{p} + \frac{dV_e}{V_o} - \frac{dm_e}{m_o}\right). \tag{36}$$

Energy balances in cooler, regenerator and heater volumes of SE are formulated as follows in Eqs. (37) to (39):

$$dQ_k = V_k \cdot dp \cdot \frac{c_v}{R} - c_p \cdot (T_{ck} \cdot m_{ck'} - T_k \cdot m_{kr'}), \quad (37)$$

$$dQ_r = V_r \cdot dp \cdot \frac{c_v}{R} - c_p \cdot (T_k \cdot m_{kr\prime} - T_h \cdot m_{rh\prime}), \quad (38)$$

$$dQ_h = V_h \cdot dp \cdot \frac{c_v}{p} - c_p \cdot (T_h \cdot m_{rh'} - T_{he} \cdot m_{he'}). \quad (39)$$

Finally, the work generation in SE is computed by Eqs. (40) to (43):

$$dW_c = p \cdot dV_c, \tag{40}$$

$$dW_e = p \cdot dV_e, \tag{41}$$

$$dW = dW_c + dW_e, (42)$$

$$W = W_c + W_e. (43)$$

The third model, curiously named Simple, also considers the heat transfer and pressure losses in the three heat exchangers of SE (heater, regenerator and cooler), especially the effectiveness of the regenerator based on parameters such as its porosity, as they significantly affect the final engine performance in terms of efficiency and generation (W). This third model is what essentially causes the different performances of SE to vary aside from the dynamic mechanism of the relative piston-displacer movement of these engines. This is due to the wide range of selections in the design of heat exchangers chosen for the heater, cooler and regenerator in this third model, which in turn is clearly dependent on the dynamic design performed.

In particular, since SE operates cyclically, the regenerator effectiveness  $\varepsilon$  is not practical in maintaining the classical definition based on the enthalpy exchange with respect to the maximum [25]. In this case, the amount of heat transferred from the gas to the regenerator in the cycle is compared with respect to the ideal adiabatic cycle,  $Q_r$ , being 0 in the worst case (no regeneration) and 1 in the best case (ideal regenerator). With a nonideal regenerator, the working gas exits from the regenerator at a lower temperature than that of the heater. Thus, non-ideal effectiveness is then traduced into an additional heat loss  $Q_{r,loss}$ , see Eq. (44), thereby increasing the temperature of the hot source of SE and decreasing the cooler one, as estimated in Eqs. (45) and (46). Typical correlations for the forced convection coefficients h in the heater and cooler were used in the MATLAB code:  $A_{w,i}$  their wetted areas.

$$Q_{r.loss} = (1 - \varepsilon) \cdot Q_r, \tag{44}$$

$$T_h = T_{wh} - \frac{(Q_h + Q_{r,loss}) \cdot f}{h_h \cdot A_{w,h}},\tag{45}$$

$$T_k = T_{wk} - \frac{(\varrho_k - \varrho_{r,loss}) \cdot f}{h_k \cdot A_{wk}}.$$
 (46)

This parameter significantly affects the thermal efficiency  $\eta$  of FPSE compared to the one obtained for the adiabatic model  $\eta_t$  [26,28], which performs the heat transfer process at constant volume, usually in a mesh, see Eq. (47):

$$\eta = \frac{\eta_i}{\left[1 + \left(\frac{Q_T}{Q_D}\right) \cdot (1 - \varepsilon)\right]}.$$
 (47)

The Simple method also considers the power loss associated with pressure drop dP in the three SE exchangers. As an example, Eq. (50) shows the associated  $dP_r$  to the regenerator.

$$dP = dP_h + dP_r + dP_k, (48)$$

$$Pump_{loss} = \int (dP \cdot dV) \cdot f, \tag{49}$$

$$dP_r = \frac{2 \cdot f_r \cdot \mu \cdot V_r \cdot G \cdot l_r}{m_r \cdot d_r^2}.$$
 (50)

It can be complemented with additional pressure losses due to the finite velocity of the piston or the internal conduction ("shuttle") losses by the regenerator [9,29], heater and cooler walls. Still, they are not included here for the sake of simplicity. Furthermore, its value is also much lower than the power reduction associated with the Simple method. For all these reasons, the Simple method is considered the closest to the real value that an SE will measure in its operation.

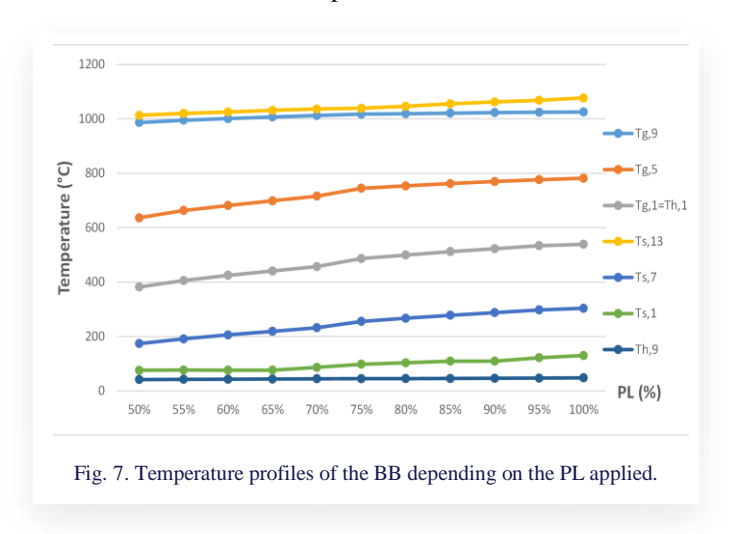
# 3. Results analysis

### 3.1. Biomass boiler

Given the complexity of solving the boiler model, which is highly sensitive to the zonal method solution and especially to the emissivity of the analyzed surfaces, the modelling of the boiler has been studied with a typical excess air for this type of boiler of 10% measured in O2 in gases, an outlet water temperature of 40°C, and an inlet water temperature depending on the partial load, which varies from 22°C to 30°C for the load range from 100% to 30%, according to the Spanish regulations regarding the certification of boiler efficiency [30]. A constant water flow rate (20 l/min) is assumed, so the outlet gas temperature is even lower at low loads since heat transmission is reduced when the gas flow rate is also reduced with the load. This temperature varies between 45°C and 49°C. This is why very similar efficiency values are obtained for this boiler throughout its possible operating range: In all cases, the thermal efficiency of the boiler yields values around 97% based on the lower heating value (LHV), which are high values and very close to condensation. Anyway, these values correspond to hot water production at a low temperature (40°C) and are consistent with the independent simulation of efficiency performed with EES.

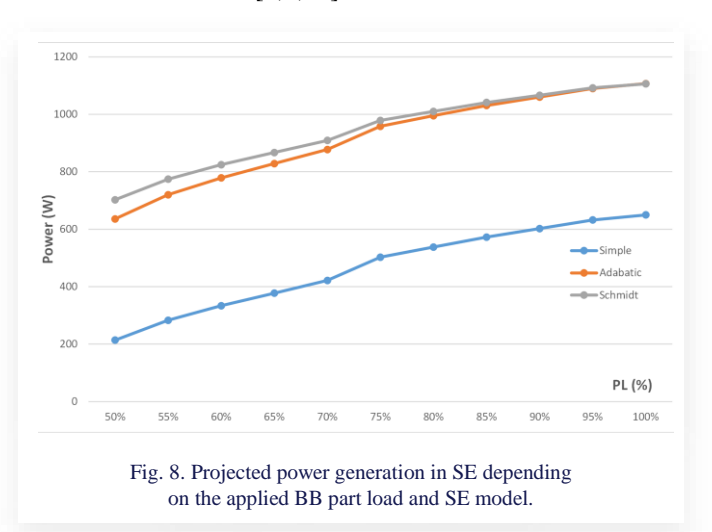
The BB modulation has only been studied from 50% to 100% in 5% variation steps, considering the subsequent connection with SE, which will require high temperatures to stay warm and produce electricity.

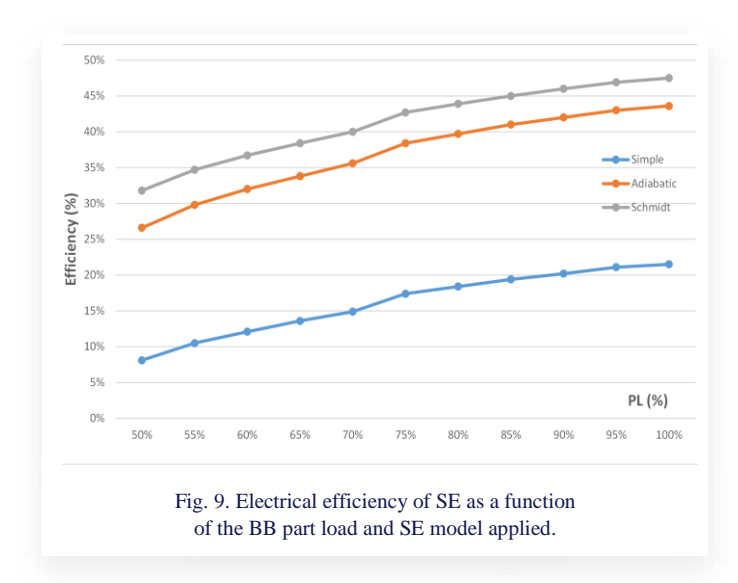
The following Fig. 7 shows some of the most relevant temperatures of the simulated model (see Fig. 2 for their location), demonstrating a clear trend based on the partial load. For example, the temperature difference  $T_{g,I}$  for the gases toward the water jacket varies by about 150°C between the minimum and maximum loads (539–382°C). It is also very interesting to analyse the temperature difference between the gas volume and its metal wall  $(T_{s,i}-T_{p,i})$ , which has 80 l of water in its jacket on the other side. A difference of 400–350°C is maintained for high loads, decreasing to 350-300°C for the lowest loads, given the lower temperatures in the combustion chamber. It can also be seen that the gas decay profile  $(T_{h,i})$  inside the jacket is much higher at the beginning than at the end of its path, and the water temperature increase  $(T_{w,i})$ , in countercurrent and upwards, heats up according to this thermal jump on the flue gas side. Regarding the actual measurements, the temperature probe is located approximately at the height of  $T_{g,2}$ ; the values obtained are very reasonable, from 597°C to 440°C. It must be said that this parameter has much higher safety limits in the commercial BB, but it is not a control parameter since the boiler is mainly controlled by the  $O_2$  measured with a lambda probe.



# 3.2. Stirling engine

The effects of the boiler performance on SE are significant in that the temperature values obtained for the heater  $(T_{s,7})$ , depending on the partial load of the BB, proportionally affect both the thermal efficiency and the expected electrical production. In calculating this temperature, there are two fundamental parameters that affect its final value: the proposed emissivity for the heater and the conduction resistance of the SE assembly. In this case, an emissivity value of 0.5 was taken for the SE heater, considering it a polished receiver but exposed to fouling from the combustion of various types of biomass. Regarding the resistance value, a figure of 0.5 K/W has been selected. This implies temperature values in the range of 190-305°C depending on the boiler load, with an electrical production in the range of 200-650 W (see Fig. 8) and increasing electric efficiencies in the order of 8-22% (simple model, see Fig. 9). Those values are comparable for the reduced number of commercial SEs. It is also evident in the previous figures that there is a reduction in production and efficiency loss as a more detailed and realistic thermodynamic model is gradually included. The difference between the isothermal and adiabatic models is that they are not so crucial in estimation of efficiency and produced power, as shown in other studies [5,9,26].





The greatest difference is shown in the jump from the adiabatic model to the simple one, where, above all, the impact of the regenerator effectiveness (about 0.6 on average) is much more significant than the power losses associated with the pressure drop of the three SE exchangers (heater, regenerator and cooler). In the same studies, the difference could also be seen.

It is important to note that heat recovery in this BB is different from other systems where the heat recovery unit is located behind the combustion chamber, and this does not favour heat capture by SE, which is the main reason for not reaching the nominal power and find relatively low heater temperatures. On the other hand, in the actual SE installation, the temperature of the cold focus will be limited by the cooling capacity of the system associated with the cooler. In this case, this effect has not been considered, and the cooling temperature taken was 300 K for the model. Although this value is less important than the heater temperature, it must be controlled within reasonable limits to have a good efficiency.

Furthermore, it should be noted that the SE heater design may vary, given the variety of models, and, in particular, the design required for the heater, considering the potential fouling that occurs during biomass combustion, which prevents the installation of fins to increase heat capture.

# 4. Conclusions

In this article, an integrated model of a biomass boiler is presented, which includes the zonal method for radiative exchange using the WSGG model and energy balances in the meshing performed for the zonal method, as well as a combustion model to estimate gas production, its composition and estimated gas and water outlet temperatures. The calculations were carried out using Excel and, subsequently, three successive EES files. The internal temperature values and the efficiency for a partial load ranging from 50% to 100% were obtained from the model.

The main advantage of this BB model is that it also provides the temperature values available in the area where the heat receiver of SE is expected to be installed. In the successive modelling of this SE in MATLAB, production values of up to 650 W and efficiencies of 22% were obtained in the best cases, assuming an emissivity of 0.5 for the engine receiver. This fig-

ure is very similar to the average production offered by a biomass boiler manufacturer that incorporates SE in its upper part.

Regarding the model error analysis, its validation is planned to be carried out shortly using experimental data obtained from the recently completed facility, including the real-time acquisition of specific measurements for both BB and SE. In any case, it will only be possible to validate some values since the real instrumentation only measures values such as  $T_{g,2}$ , the temperatures of the gas  $(T_{h,9})$  and water inlet and outlets  $(T_{w,9}, T_{w,1})$  in BB, and the temperature of the SE head  $(T_{s,7})$  in the SE controller. It should also be made clear that the model is a simplification of the actual installation since SE will have a specific vertical movement and, therefore, the combustion chamber will not be precisely a cylinder, which gives it a particular uncertainty associated with the validation due to these undesirable geometrical effects. Since the BB model is based on a zonal radiation model, it depends on the meshing used to create it. According to Larsen and Howell [31], the maximum error in temperatures or heat fluxes is less than 1.5% for a similar meshing example. In the case of SE, the articles mentioned in section 3.2 have found an error relative to a real SE of around 3-4% in the best cases. With all reservations, the model is expected to yield an error of less than 10% in the experimental measurements taken.

This model is more flexible than the actual installation as it allows for modification of aspects that are not feasible in said installation, and therefore, once validated, can be a way of proposing improvements to the installation because of the results. In any case, it is necessary to comment that the sequential model is very sensitive. Any modification of a substantial parameter in the model requires recalculating all downstream modules from the modified one till its convergence. Nevertheless, certain parameters have already been identified as crucial in these models, such as:

- The emissivities  $\varepsilon$  of the internal surfaces of the boiler enclosure, especially that of SE and the surface where combustion (flame,  $T_{s,13}$ ) takes place;
- The treatment of the area adjacent to the burner outside the
  irradiated enclosure. Currently, it has been considered that
  there is no participatory medium in the radiation between
  the inner walls of BB (*T<sub>s,i</sub>*) and the outer walls of the water
  jacket (*T<sub>p,i</sub>*);
- The thermal resistance is assumed for the entire SE assembly since, in the energy balance of the combustion chamber, it is a relevant loss that greatly affects the value obtained from *T*<sub>s,7</sub> (input of the SE model);
- The excess air in combustion would vary the gas temperature profiles and thus produce less (or more) hot water and electricity from this hybrid system;
- The section considered for the exit of combustion gases in the burner involves the treatment of gaseous convection in the internal boiler enclosure, which is very sensitive to existing passage sections.

The ultimate goal is to produce enough power from this boiler, making it a self-sufficient system in isolated and wooded areas where solar resources are scarce but biomass is abundant. This can be achieved by maintaining the SE head temperature above 350°C.

# **Acknowledgements**

This publication is part of the R+D+i project ENSURE (TED2021-131397B) funded by MCIN/AEI/10.13039/501100011033/ and European Union NextGenerationEU/PRTR.

### References

- [1] Schneider, T., Müller, D., & Karl, J. (2020). A review of thermochemical biomass conversion combined with Stirling engines for the small-scale cogeneration of heat and power. *Renewable and Sustainable Energy Reviews*, 134, 110288. doi: 10.1016/j.rser. 2020.110288
- [2] Zhu, G., Yu, K., Liang, W., Dai, W., & Luo, E. (2021) A review of Stirling-engine-based combined heat and power technology. *Applied Energy*, 294, 116965. doi: 10.1016/j.apenergy.2021. 116965
- [3] Hachem, H., Gheith, R., Aloui, F., & Nasrallah, S.B. (2018) Technological challenges and optimization efforts of the Stirling machine: A Review. *Energy Conversion and Management*, 171, 1365-1387. doi: 10.1016/j.enconman.2018.06.042
- [4] Zare, S., & Tavakolpour, A. (2020) Free piston Stirling engines: A review. *International Journal of Energy Research*, 44, 5039–5070. doi: 10.1002/er.4533
- [5] Ahmadi, M.H., Ahmadi, M.A., & Pourfayaza, F. (2017) Thermal models for analysis of performance of Stirling engine: A review. *Renewable and Sustainable Energy Reviews*, 68, 168–184. doi: 10.1016/j.rser.2016.09.033
- [6] Jiménez, P., Cardozo, E., Choque, L.A., & Araoz, J.A. (2020) Performance Analysis of a Stirling Engine Hybrid Power System. *Energies*, 13, 980. doi: 10.3390/en13040980
- [7] Laazaar, K., & Boutammachte, N. (2020) New approach of decision support method for Stirling engine type choice towards a better exploitation of renewable energies. *Energy Conversion and Management*, 223, 113326. doi: 10.1016/j.enconman.2020. 113326
- [8] Udeh, G.T., Michailos, S., Ingham, D., Hughes, K.J., Ma, L, & Pourkashanian, M. (2020) A techno-enviro-economic assessment of a biomass fuelled micro-CCHP driven by a hybrid Stirling and ORC engine. *Energy Conversion and Management*, 227, 113601. doi: 10.1016/j.enconman.2020.113601
- [9] Auñón, J.A., Pérez, J.M., Martín, M.J., Auñón, F., & Núñez, D. (2023) Development and validation of a software application to analyse thermal and kinematic multimodels of Stirling engines. *Helyon*, 9, 18487. doi: 10.1016/j.heliyon.2023.18487
- [10] Jiang, Z., Yu, G., Zhu, S., Dai, W., & Luo, E. (2022) Advances on a free-piston Stirling engine-based micro-combined heat and power system. *Applied Thermal Engineering*, 217, 119187. doi: 10.1016/j.applthermaleng.2022.119187
- [11] Kwankaomeng, S., Silpsakoolsook, B., & Savangvong, P. (2014) Investigation on Stability and Performance of a Free-Piston Stirling Engine. *Energy Procedia*, 52, 598–609. doi: 10.1016/j. egypro.2014.07.115
- [12] González-Pino, I., Pérez-Iribarren, E., Campos-Celador, A., Terés-Zubiaga, J., & Las-Heras-Casas, J. (2020) Modelling and experimental characterization of a Stirling engine-based domestic micro-CHP device. *Energy Conversion and Management*, 225, 113429. doi: 10.1016/j.enconman.2020.113429
- [13] Valenti, G., Campanari, S., Silva, P., Fergnani, N., Ravidà, A., Di Marcoberardino, G., & Macchi, E. (2014) Modeling and testing of a micro-cogeneration Stirling engine under diverse conditions of the working fluid. *Energy Procedia*, 61, 484–487. doi: 10.1016/j.egypro.2014.11.1154

- [14] Choque, L.A., & Araoz, A. (2023) A Case Study of the Development Experience of Using a Prototype Stirling Engine in A Novel Bioenergy Driven Co-Generation Plant in Bolivia. *Heat Transfer Engineering*, doi: 10.1080/01457632.2023.2185492
- [15] Cardozo, E., Erlich, C., Malmquist, A., Jiménez, & Alejo L. (2014). Integration of a wood pellet burner and a Stirling engine to produce residential heat and power. *Applied Thermal Engine-ering*, 73, 671–680. doi: 10.1016/j.applthermaleng.2014.08. 024
- [16] Damirchi, H., Najafi, G., Alizadehnia, S., Mamat, R., Sidik., N. A.C. Azmi, W.H., & Noor M.M. Micro Combined Heat and Power to provide heat and electrical power using biomass and Gamma-type Stirling engine. *Applied Thermal Engineering*, 103, 1460–1469. doi: 10.1016/j.applthermaleng.2016.04.118
- [17] Arashnia, I., Najafi, G., Ghobadian, B., Yusaf, T., Mamat, R., & Kettner, M. (2015) Development of micro-scale biomass-fuelled CHP system using Stirling Engine. *Energy Procedia*, 75, 1108–1113, doi: 10.1016/j.egypro.2015.07.505
- [18] Cardozo, E., & Malmquist, A. (2019) Performance comparison between the use of wood and sugarcane bagasse pellets in a Stirling engine micro-CHP system. *Applied Thermal Engineering*, 159, 113945, doi: 10.1016/j.applthermaleng.2019.113945
- [19] Araoz, J.A., Cardozo, E., Salomon, M., Alejo, L., &. Fransson, T.H. (2015) Development and validation of a thermodynamic model for the performance analysis of a gamma Stirling engine prototype. *Applied Thermal Engineering*, 83, 16–30. doi: 10.1016/j.applthermaleng.2015.03.006
- [20] Esteban, I. (2014) Análisis y caracterización de la combustión de pélets en una caldera Solarfocus TII30 de llama invertida. Universidad de Valladolid (in Spanish).
- [21] Hottel, H.C., & Sarofim, A.F. (1967) *Radiative Transfer*. McGraw Hill Book Company, New York.
- [22] Noble, J.J. (1975) The zone method: Explicit matrix relations for total exchange areas. *Int. J. Heat Mass Transfer*, 18, 261-269.
- [23] Hofgren, H., & Sunden, B. (2015) Evaluation of Planck mean coefficients for particle radiative properties in combustion environments. *Heat Mass Transfer*, 51, 507–519. doi: 10.1007/s00231-014-1431-0
- [24] Rhine, J.M., & Tucker, R.J. (1991) Modelling of gas-fired furnaces and boilers and another industrial processes. British Gas plc.
- [25] Walker, G., & Senft, J.R. (1985) Free Piston Stirling Engines. (1st ed.). Springer-Verlag.
- [26] Urieli, I., & Berchowith, D.M: (1984) *Stirling Cycle Engine Analysis*. Adam Hilger Ltd.
- [27] Urieli, I. (2002) Stirling Cycle Machine Analysis. https://www.ohio.edu/mechanicalfaculty/urieli/stirling/Index.html [accessed 28 September 2023].
- [28] Scarpin, G. (2012) *Modelo Simple de Motores Stirling*. Informe Técnico: DMA-012/12. Instituto Universitario Aeronáutico, Córdoba, Argentina (in Spanish).
- [29] Araoz, J.A., Salomon, M., Alejo, L., & Fransson, T.H. (2014) Non-ideal Stirling engine thermodynamic model suitable for the integration into overall energy systems. *Applied Thermal Engine-ering*, 73, 205–221. doi: 10.1016/j.applthermaleng.2014.07. 050
- [30] CTE UNE124 (2023) Generadores y emisores de calor. Norma Española UNE-EN 303-5:2022+A1. Heating boilers. Part 5: Heating boilers for solid fuels, manually and automatically stoked, nominal heat output of up to 500 kW. Terminology, requirements, testing, and marking. Madrid (in Spanish).
- [31] Larsen, M.E., & Howell, J.R. (1985) The Exchange Factor Method: An Alternative Basis for Zonal Analysis of Radiation Enclosures. *Journal of Heat Transfer*, 107(4), 936–942. doi: 10.1115/1.3247524